Chapter-IV

Characterization Studies

This chapter includes the results of characterization studies of all the samples of three different series. The samples were characterized by X-ray diffraction, Differential scanning Calorimetry, Fourier Transform Infrared Spectrometry, transport number measurement by EMF method and Density measurement by Archimedes's Principle .

4.1 X-Ray Diffraction Studies:

X-ray diffraction measurements were carried out in order to determine the amorphous nature of the present samples. Absence of well defined peak in the x-ray diffraction spectra characterizes the glassy state [1, 2].

X-ray diffraction spectrum for the glass samples of first series, $x(BaO:1.5Ag_2O)$-$(95-x)V_2O_5$-$5TeO_2$, where the modifier ratio is varying from 25 to 45 in steps of 5 are shown in Fig. 4.1 at room temperature. The observed peak free pattern shows the absence of any crystalline phase which confirms the amorphous nature of the samples. These patterns show a broad halo at $2\theta \sim 27.5^0$, beyond that no further oscillations are observed. The intensity of these halos differs in height as a function of (BaO-Ag_2O) content in the specimens. It is very weak for x=25 % sample but it develops to a sharper halo as the modifier content increases, reaching a maximum at the x=45 mol %. Thus, the XRD spectrum confirms the amorphous nature of the glass samples of first series. Fig.4.12 shows the XRD pattern of all glass samples of second series 10 BaO-yAg_2O-$(85-y)$ V_2O_5-$5TeO_2$, obtained at room temperature. These patterns show two very feeble humps at $2\theta = 15^0$ and 55^0, whose intensity increases slightly with increasing Ag_2O content. A broad hump is observed at $2\theta = 28^0$. The intensity of this hump increases with increasing Ag_2O content and is shifted to a position $2\theta = 30^0$ for 50 and 55 % sample. The intensity of this hump is very weak for y=20 % and develops to a sharper but very broad peak like hump for y=55 %. No crystalline phases are present which confirms the amorphous nature of the samples of this system too. Fig.4.13 shows the XRD pattern for third series samples at room temperature. In this series, BaO and V_2O_5 content are kept constant and Ag_2O is varied with

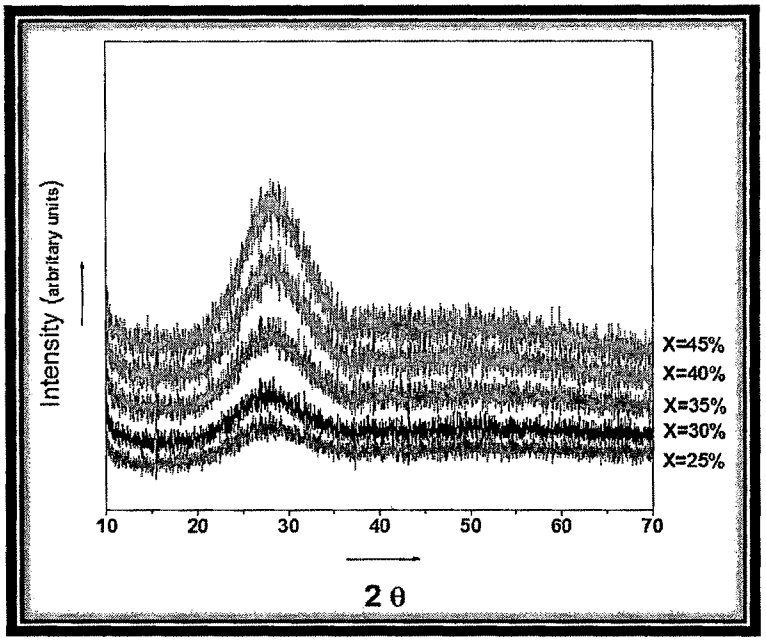

Fig.4.1. XRD diffraction pattern of x(BaO:1.5Ag_2O)-(95-x)V_2O_5-5TeO_2.

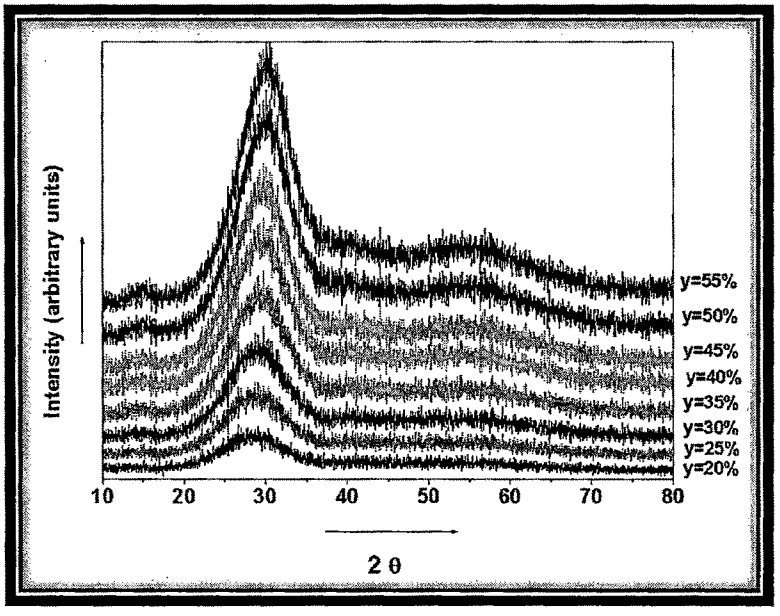

Fig.4.12. XRD diffraction pattern of 10BaO-yAg_2O-(85-y)V_2O_5-5TeO_2.

respect to TeO_2 content. The peak free amorphous pattern of XRD spectrum shows two small humps at $2\theta = 15^0$ and 55^0, whose intensity increases very

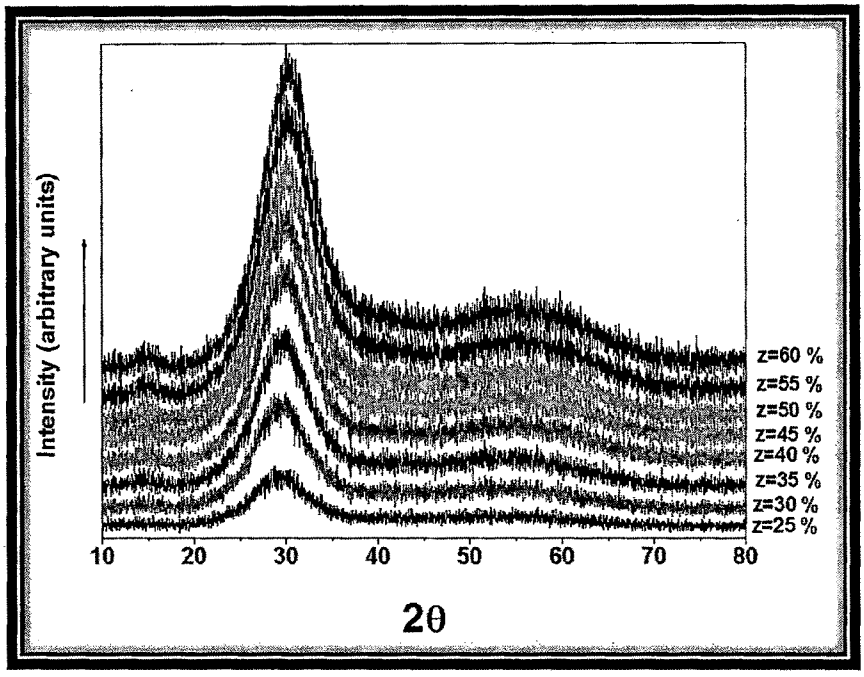

Fig.4.13. XRD diffraction pattern of $5BaO\text{-}zAg_2O\text{-}35V_2O_5\text{-}(60\text{-}z)TeO_2$.

slightly with increasing Ag_2O content. A broad hump is observed at $2\theta = 29^0$. The intensity of this hump also increases with increasing Ag_2O content and becomes maximum for highest Ag_2O content i.e., z= 60 mol % similar to the diffraction pattern obtained for the samples in second series.

From the above observation, it is clear that these glass samples are amorphous in nature as confirmed by their XRD spectrum which reveal the peak free pattern i.e., no phase of crystallinity.

4.2 Differential Scanning Calorimetry:

In order to show that all the prepared samples were indeed glasses, they were analyzed by DSC technique. It measures the temperature and heat flow associated with the transition in materials as a function of time and temperature. The DSC measurements were used to determine the glass transition temperature (T_g) in order to establish an upper limit of temperature to perform the conductivity measurements and to avoid any structural relaxations and/or crystallization due to glass-liquid transition.

In the DSC plot [Fig.2.4], the x-axis represents the temperature and the y-axis represents the difference in heat flow between the sample and the reference. The number, shape and position of the various endothermic and exothermic peaks with reference to the temperature may be used as a means for the qualitative identification of the substance under investigation. When the sample and the reference material are heated, the heat is either absorbed or released by the material against temperature due to phase change or crystallization or change in heat capacity. When the horizontal line in the DSC spectrum shifts downward suddenly at a certain temperature, it means heat is being absorbed by the sample or a change in its heat capacity. This particular temperature is known as *"glass transition temperature"* T_g. Another endothermic peak is observed at a very high temperature known as *"liquidus or melting temperature"* T_m. At this temperature the chains come out of their ordered arrangements and begin to move around freely. When the substance melts, it must absorb heat.

Above the glass transition, the substance has lot of mobility. When they reach the right temperature, they will gain enough energy to move into an ordered

arrangement called crystals. When the substance fall into these crystalline arrangements or when the substance undergoes from metastable to crystalline state, they give off heat and it is seen as an exothermic peak in the plot of heat flow versus temperature. The temperature at this highest point is usually considered to be the crystallization temperature of the sample. The substance gives off heat when it crystallizes; it is called an exothermic transition. Limb and Davis [3] reported that for V_2O_5-P_2O_5-B_2O_3 glass system, there are two phase transition separation and subsequent crystallization of V_2O_5 is at 290^0C and 410^0C. In glass transition, there is no peak, because there is no latent heat given off, or absorbed, by the substance. Both melting and crystallization involve absorbing or giving off heat. At the glass transition temperature, there is a change in the heat capacity of the sample and there is no latent heat involved. Hence the glass transition is called as second order transition. Transitions like melting and crystallization, which do have latent heats, are called first order transitions.

DSC plot obtained for all samples of first series x (BaO:1.5 Ag_2O)-(95-x) V_2O_5-5 TeO_2 with $25 \leq x \leq 45$, are shown in Fig. 4.14. These plots show an endothermic peak corresponding to glass transition temperature (T_g) and an exothermic peak corresponding to cryatsllization temperature (T_c). The values of glass transition temperature obtained from these plots are plotted against modifier content (BaO:1.5 Ag_2O) as shown in Fig. 4.15. The figure clearly indicates that the glass transition temperature is independent of the modifier content. Similar independence nature of glass transition temperature with respect to modifier is also obtained in MgO-V_2O_5 glasses [4] but some workers [5, 6] have shown that glass transition temperature increases with decrease in V_2O_5 content.

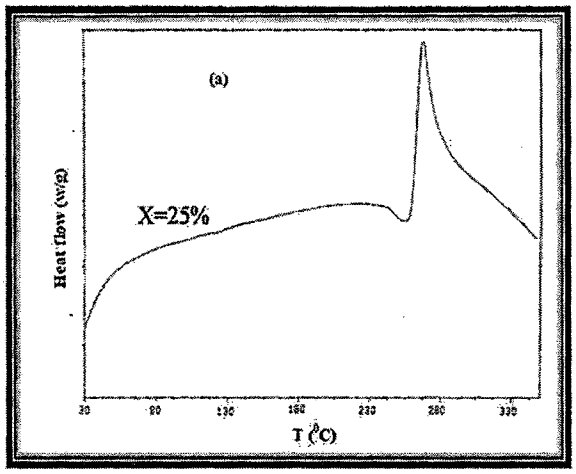
(a)
X=25%
Heat flow (w/g)
T (°C)

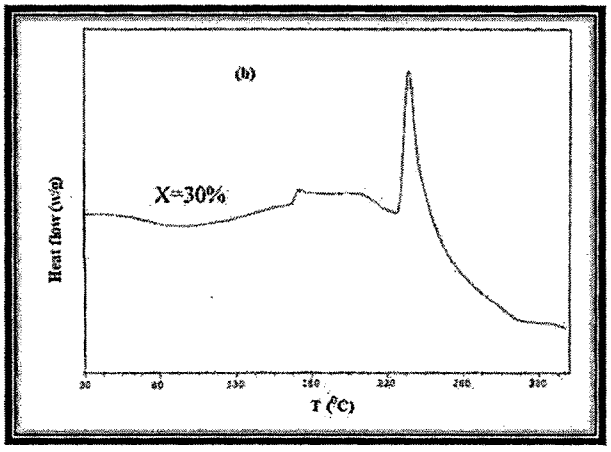
(b)
X=30%
Heat flow (w/g)
T (°C)

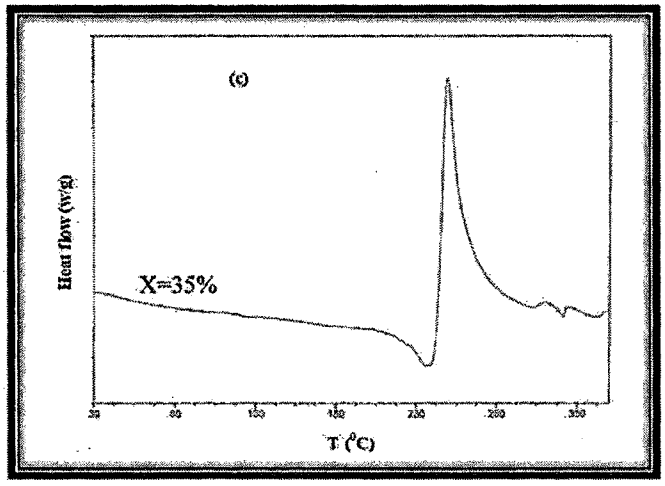
(c)
X=35%
Heat flow (w/g)
T (°C)

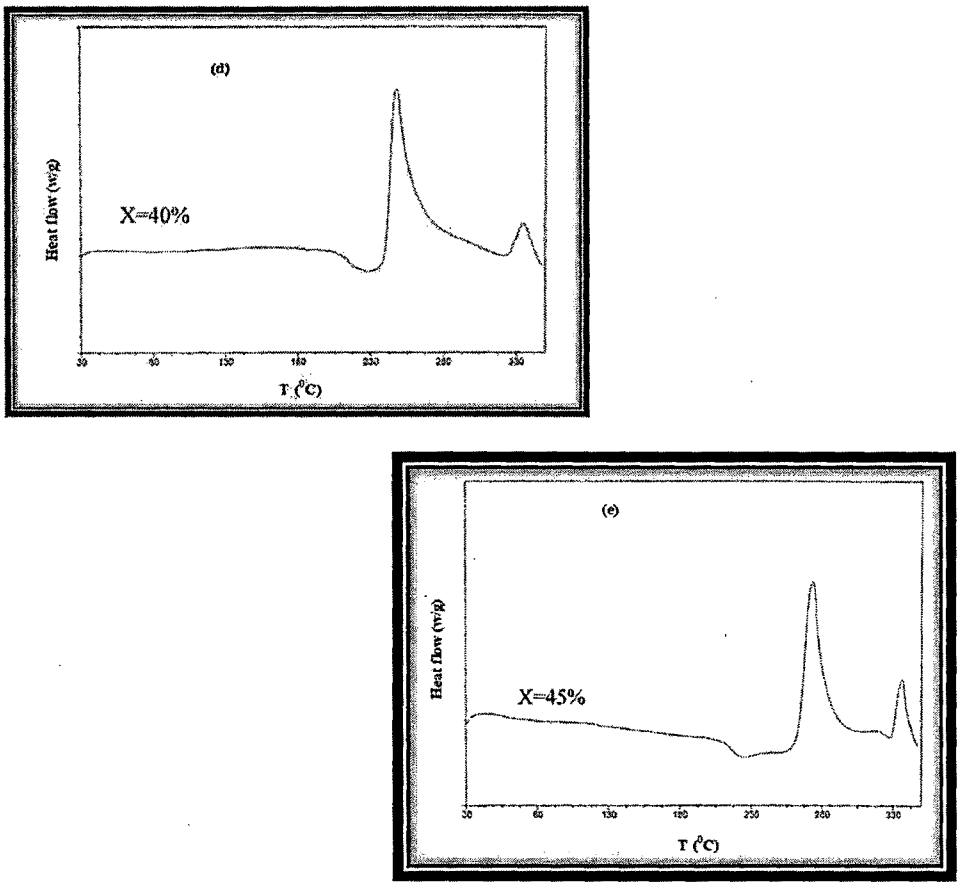

Fig.4.14. DSC traces for all samples of series x(BaO:1.5Ag$_2$O)-(95-x)V$_2$O$_5$-5TeO$_2$.

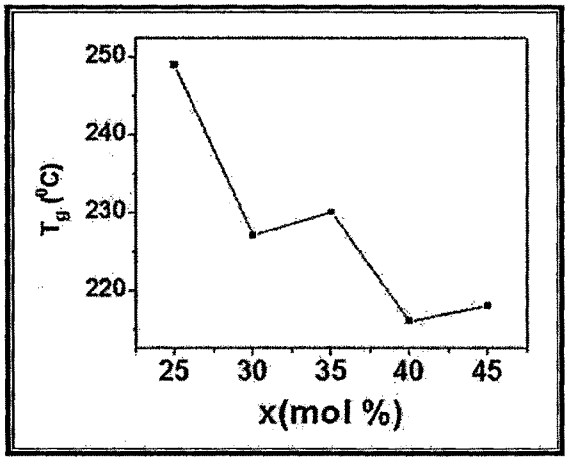

Fig.4.15. Variation of glass transition temperature T_g with modifier in series x(BaO:1.5Ag$_2$O)-(95-x)V$_2$O$_5$-5TeO$_2$.

Fig.4.16 shows the DSC thermogram obtained for different glassy compositions of the second series 10 BaO-y Ag_2O-(85-y)V_2O_5-5TeO_2 with $20 \leq y \leq 55$, in steps of 5 mol %. The obtained T_g values are plotted with Ag_2O content shown in Fig. 4.17, which shows that the glass transition temperature decreases with increasing Ag_2O content. Double or triple exothermic peaks, present in some glass compositions represent multiple crystalline phases appearing during heating up. More than one exothermic peak is reported in other tellurite glasses also [7].

DSC results of third series 5 BaO-z Ag_2O-35 V_2O_5-(60-z)TeO_2 with $25 \leq z \leq 60$ are shown in Fig.4.18. It shows endothermic dip due to glass transition and crystallization of the samples is shown by exothermic peaks. The thermographs of this series also show double and triple exothermic peaks, as seen in second series,

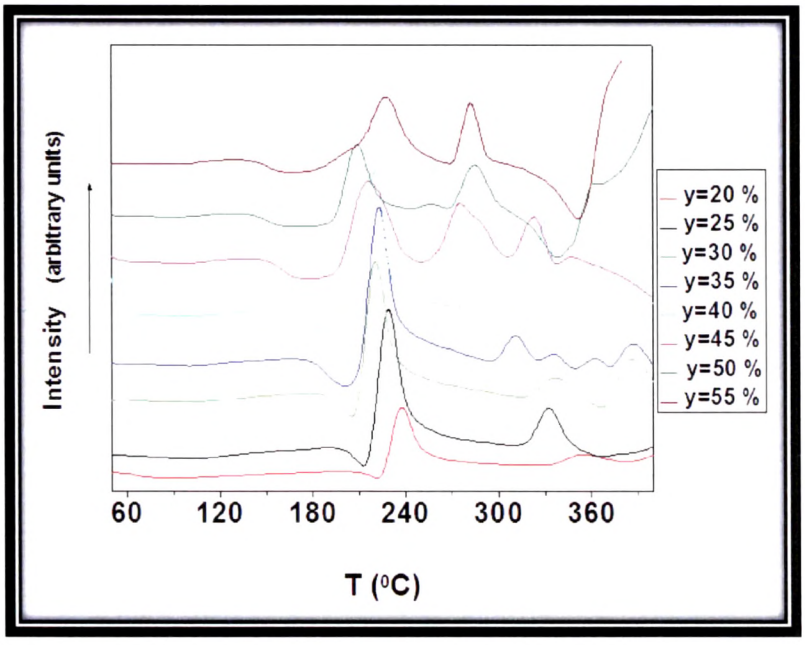

Fig.4.16. DSC traces of all samples of series 10BaO-yAg_2O-(85-y)V_2O_5-5TeO_2.

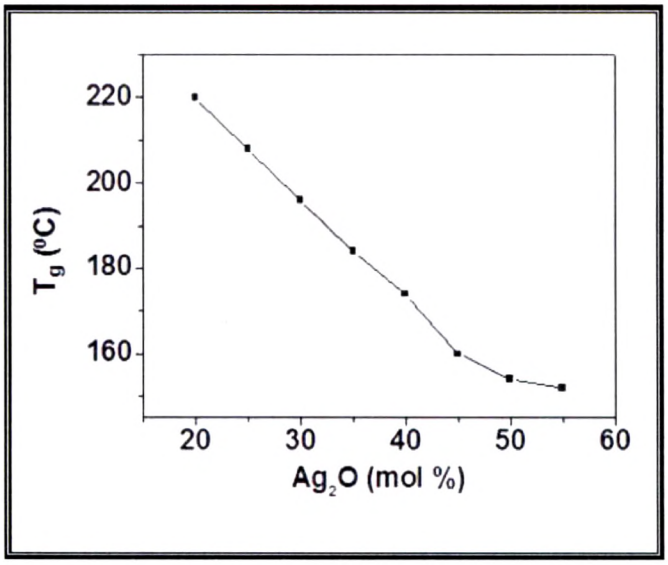

Fig.4.17. Variation of glass transition temperature T_g with modifier Ag_2O in 10BaO-yAg_2O-(85-y)V_2O_5-5TeO_2 series.

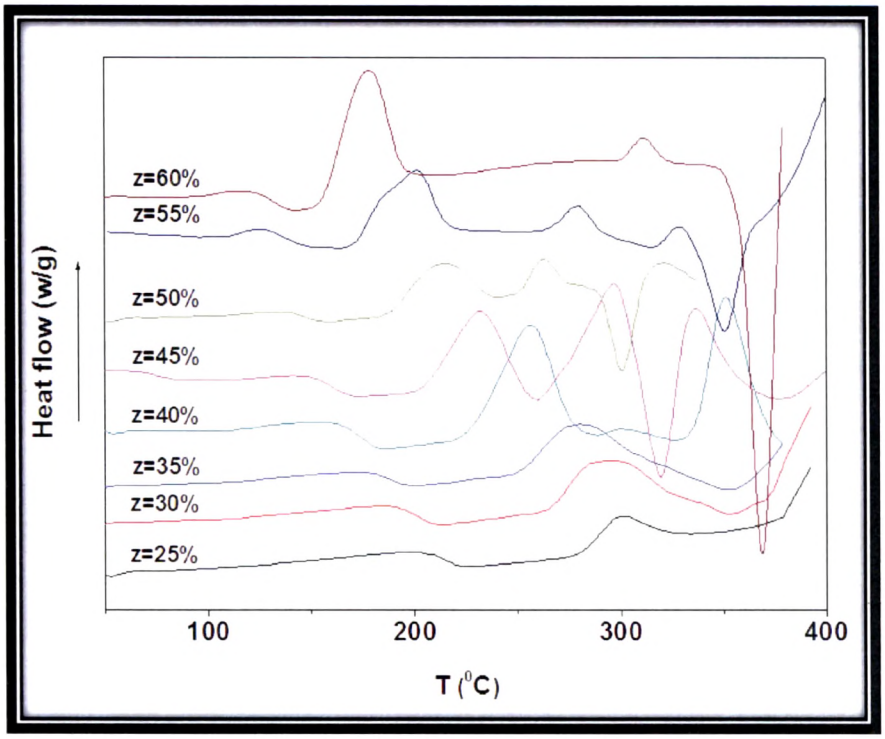

Fig.4.18. DSC traces of all samples of 5BaO-zAg_2O-35V_2O_5-(60-z)TeO_2 series.

due to different crystalline phases appearing due to heating up. The glass transition temperature (T_g), obtained from the DSC spectrum of this series are plotted against modifier content Ag_2O, as shown in Fig.4.19. This figure clearly shows that T_g decreases with increasing modifier content (Ag_2O), similarly as observed in second series. The decrease in T_g with increasing modifier content (Ag_2O) in the samples of second and third series suggests that a larger number of bonds are destroyed within the glassy network because the Ag^+ ion goes to interstitial sites which opens up the structure to form a more open type thermodynamically stable and amorphous phase.

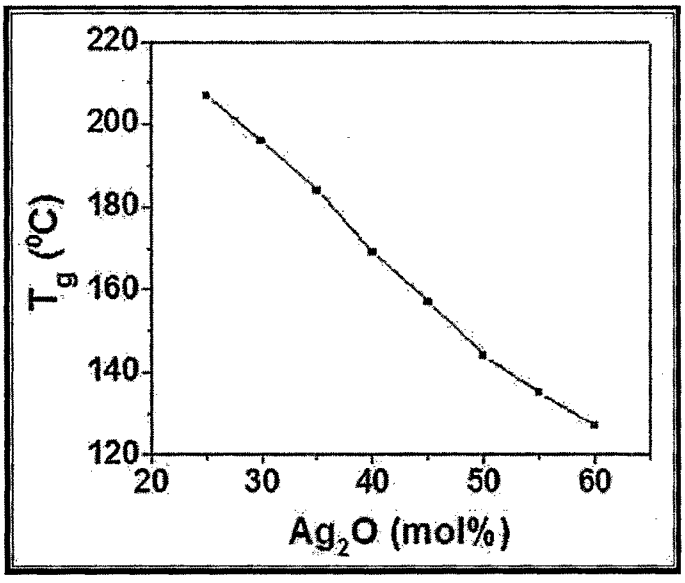

Fig.4.19. Variation of glass transition temperature T_g with modifier Ag_2O in 5BaO-zAg_2O-35V_2O_5-(60-z)TeO_2 series.

4.3 Fourier Transform Infrared Spectroscopy:

FTIR technique is a powerful tool to investigate the structural details of materials. IR spectra of the present glasses provide information about the types of vanado-tellurite structural units and the change due to the variation of modifier and glass formers. The FTIR spectrum of pure crystalline V_2O_5 is shown in Fig.4.20 which shows the presence of 1020, 830, 620 and 490 cm^{-1} absorption bands. The V_2O_5 structure is built up by deformed VO_5 trigonal bonded in zigzag chains. Each VO_5 group contains a short V=O bond (vanadyl group) [8].The sharp band at 1020 cm^{-1} is assigned to the vanadyl group of V=O bond where as vibrations at 830 cm^{-1} is related to asymmetric stretching vibrations along V-O-V chain involved in

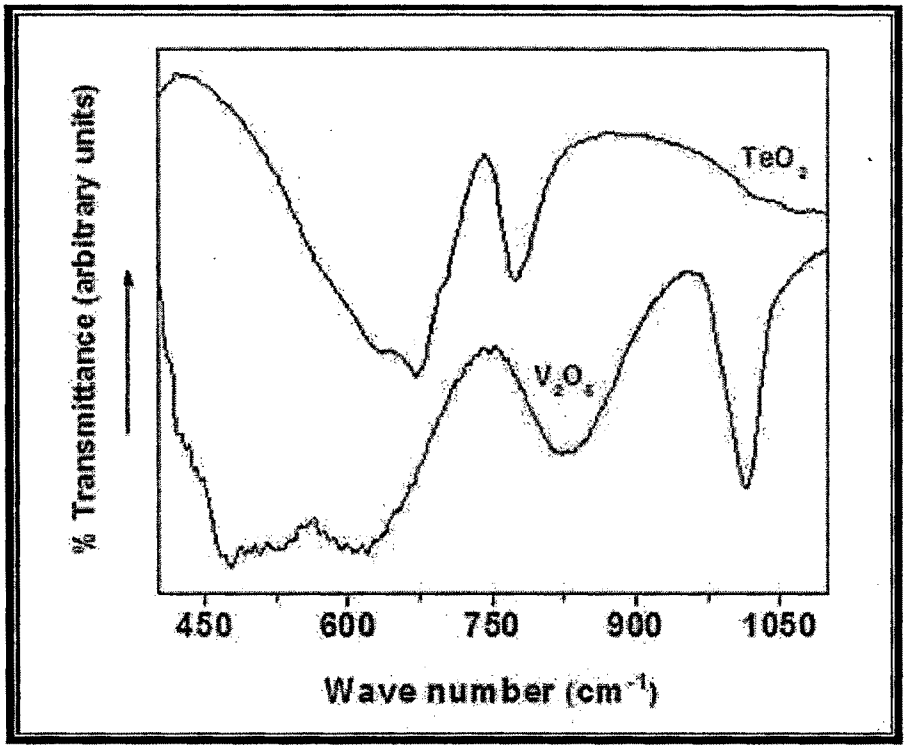

Fig.4.20. FTIR spectra of pure TeO_2 and V_2O_5.

corner sharing of VO_5 polyhedral [7]. Absorption band present at 620 cm^{-1} corresponds to V-O-V bond of symmetrical stretching and the band at 490 cm^{-1} arises from the bending modes of V-O-V group.

Fig.4.20 also shows the FTIR spectrum of pure crystalline TeO_2 which has characteristic features at 632, 669 and 773 cm^{-1}. These absorption bands correspond to stretching vibrations of the Te-O bonds. The bands at 632 and 669 cm^{-1} are assigned to ν_{axial}^{sym} and ν_{axial}^{asym} modes of TeO_4 groups while the band at 773 cm^{-1} is assigned to $\nu_{equatorial}^{sym}$ vibrations of TeO_4 group [9]. Thus, low frequency bands are due to axial mode while the high frequency band is assigned to equatorial mode vibrations.

The FTIR spectra of the samples of the first series x (BaO: 1.5 Ag_2O)- (95-x)V_2O_5-5TeO_2 where $25 \leq x \leq 45$, in steps of 5 are shown in Fig.4.21. The main feature of the spectrum is the appearance of the resonance peaks at 960 cm^{-1}, 894 cm^{-1} and 630-750 cm^{-1} and the broadening of the absorption bands, which is attributed to the random network and lack of long range order [10]. The small kink observed at position 960 cm^{-1} is attributed to V=O bonds in glasses which appears at 1020 cm^{-1} in pure V_2O_5 spectra (Fig.4.20). It is known that added Ba^{+2} ions [11] or Ag^{+} ions modify the network by occupying interstitial sites in these glasses; each added modifier oxide (Ba^{+2}/Ag^{+}) gives rise to the formation of non-bridging oxygen there by creating V-O^{-} units. The oxygen which becomes non-bridging and acquires a negative charge will move closer to the connected vanadium ion, in effect reducing the positive charge on the vanadium ions and there by resulting in a decrease in the binding of other oxygen attached to this particular ion; the length of the V=O bond therefore increases. It is known that the

V_2O_5 network structure is mainly build up of VO_5 polyhedra for the glass compositions with lower amount of modifier [12]. However, as V_2O_5 content decreases and modifier increases the glass structure consists of VO_4 polyhedra as well [12-14]. Thus, the shifting of V=O bond with increasing modifier content towards lower wave number, in IR spectrum, implies that Ba or Ag ions in these compositions are located between vanadate chains and layers and the glass structure consists of VO_4 polyhedra [15].

With further addition of modifier, the band at 960 cm^{-1} is disappeared and shows a broad band at 894 cm^{-1} which is assigned to the VO_3 terminal stretching of the

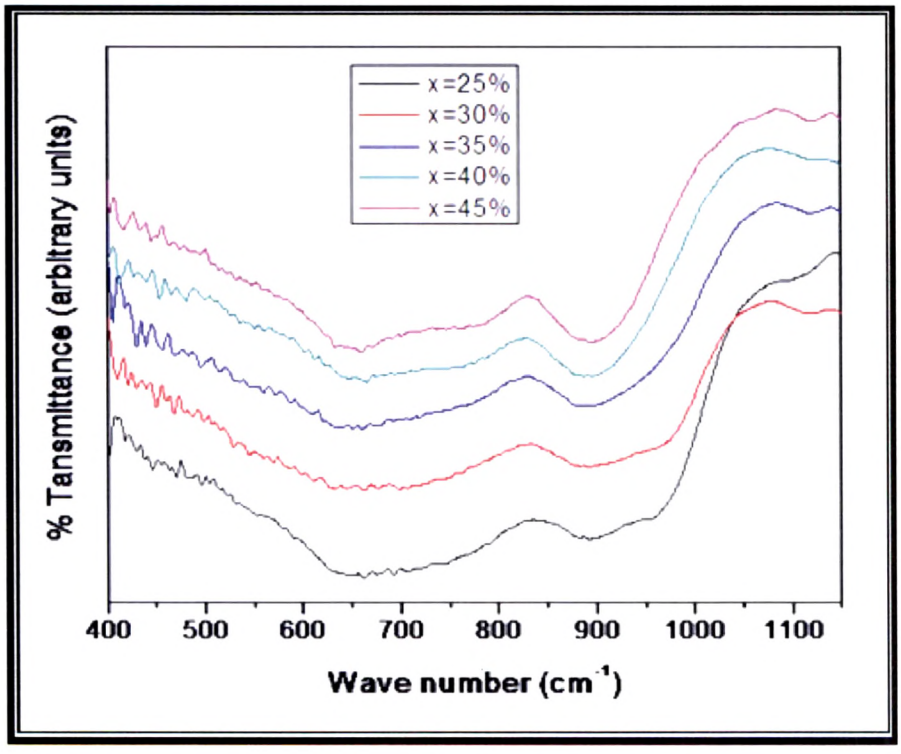

Fig.4.21. FTIR spectra of all samples of x(BaO:1.5Ag_2O)-(95-x)V_2O_5-5TeO_2 series.

pyrovanadate ions. Pyrovanadate structural units can be viewed as condensed macro anion clusters of VO_4^{-3} tetrahedra. The intensity of this band increases with increasing modifier oxides. A very broad absorption band is observed in 630-780 cm^{-1} range, which may be due to the symmetric vibrations of V-O-V group (normally observed at around 620 cm^{-1}) or TeO_4 group (observed at around 632 and 669 cm^{-1}). A very small dip is seen for x=40 and 45 % samples at 780 cm^{-1} which may be due to ν_{asym} vibrations of V-O-V bonds involved in the corner sharing of VO_5 polyhedra [16] which is shifted towards lower wave numbers due to the increasing modifier (BaO and Ag_2O). Generally, a vibrational band due to TeO_3 group is also expected near 770 cm^{-1}. Hence, the peak near to 780 cm^{-1} may be due to the combined effect of asymmetric vibrations of V-O-V and TeO_3 groups.

Fig.4.22 shows the FTIR spectra for the samples of second series 10 BaO-yAg_2O-(85-y)V_2O_5-5TeO_2 glass system. In this series, the amount of Ag_2O is increasing from 20 to 55 mol % whereas V_2O_5 is decreasing from 65 to 30 mol %. BaO and TeO_2 are kept constant in this series at 10 and 5 mol % respectively. The infrared absorption spectrum shows different bands at 1020, 964, 920, 895, 866, 850, 825, 777, 750, 669, 498, 469 cm^{-1} for different glass samples.

The structural pattern of tellurium containing glasses is determined by trigonal pyramids [TeO_3] and bipyramids [TeO_4], whose unusual structure causes the emergence of an intermediate coordination state of tellurium ions 3+1 [9]. The Te atoms are connected at vertices by Te-O-Te [17] and Te-O-V linkages which may connect the VO_5 and TeO_4 or TeO_3 polyhedra. On Adding Ag_2O in the system, oxygen species such as Te-O-Te, V-O-V, V=O, Te=O, Te-O-V, V-O-Ag^+, Te-O^-

Ag^+ may be present in the glass system [18]. XPS studies for Ag_2O-V_2O_5-TeO_2 system [18] shows the presence of various tellurium structural units, which include TeO_4, $(TeO_3)^-$, $(TeO_3)^{-2}$, TeO_{3+1}, $(Te_2O_5)^2$ and Te-Ag. The Ag-Te bond is formed when Ag_2O content is ≥ 30 mol %. The absorption of TeO_3 groups has a higher frequency position than TeO_4 groups; however this difference is insignificant due to the manifestation of the intermediate coordination state of tellurium ion 3+1. For the samples y=20, 25, 30 mol%, the band at position 469 cm^{-1} is assigned to Te-O-V bond, whose intensity decreases continuously and is absent for y=35-55 mol % sample, while the band at 669 cm^{-1} is attributed to TeO_4 [19] group and 750 cm^{-1} is attributed to TeO_3 group. For y= 45, 50, 55 mol % samples this band is slightly shifted and a broad band occurs at position 777 cm^{-1} which is attributed to TeO_3 structural units [20]. The characteristic vibrations of the isolated vanadium oxygen bonds in the IR spectrum are in the range of 1020-900 cm^{-1} [21]. The band at 1020 cm^{-1} is related to the vibrations of the non-bridging V=O of the VO_5 groups [22]. The intensity of this band decreases with decreasing V_2O_5 content but the position remains unchanged. There is a change in the band position from y=35 mol % sample.

Some new bands start forming for y= 40 to 55 mol % samples at position 498, 850, 895 and 964 cm^{-1}. For y=35 mol % sample, two absorption bands occurs at position 825 and 866 cm^{-1} which is absent for other samples and gives high intensity absorption band at 850 cm^{-1} for y=40 to 55 mol % samples. This band is attributed to the asymmetric vibrations along the V-O-V bonds involved in the corner sharing of VO_5 polyhedra [23].

For y=40 to 55 mol % samples, the band at position 498 cm^{-1} is assigned to ν_{sym}

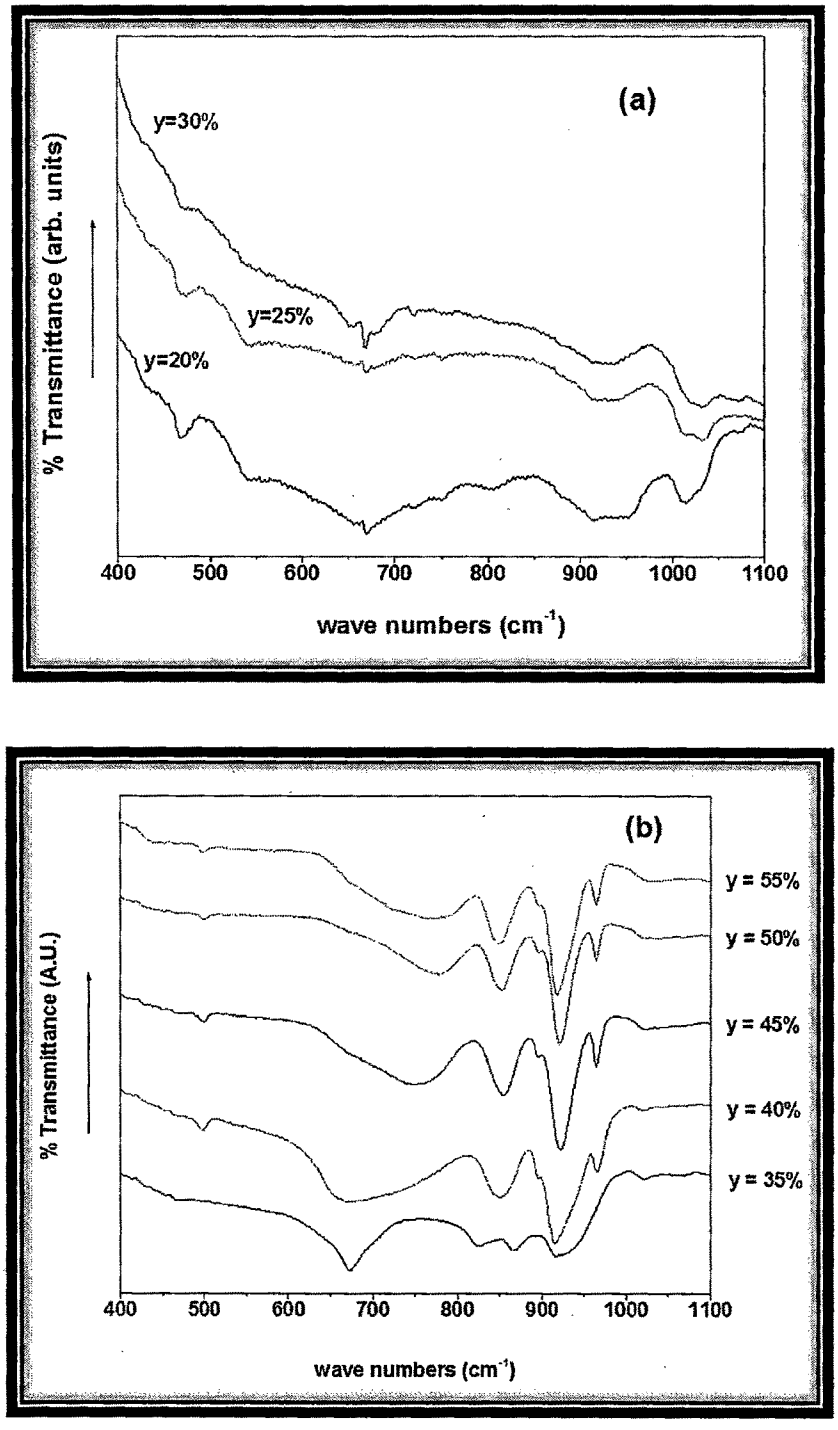

Fig.4.22: FTIR spectrum of the series 10 BaO-yAg_2O-(85-y)V_2O_5-5TeO_2 for (a) for y=20, 25 and 30 mol % & (b) for y=35, 40, 45, 50 and 55 mol%.

stretching vibrations of V-O-V bridge of $V_2O_7^{-4}$ groups [24]. The band at 895 and 920 cm^{-1} is assigned to VO_3 terminal stretching of the pyrovanadate ions and 964 cm^{-1} band is assigned to symmetric stretching vibrations of the VO_2 groups of the VO_4 polyhedra [25]. Arof [26] observed the same band position in the IR spectrum for Ag_2O-V_2O_5 and AgI-Ag_2O-V_2O_5 system. He concluded from the spectrum that the AgI acts as a plasticizing agent, as in polymer diluents system and does not interact with the Ag_2O-V_2O_5 network.

Similarly, in the third series 5 BaO-zAg_2O-35V_2O_5-(60-z) TeO_2 where z=25 to 60 in steps of 5, the IR spectra has been taken to understand the effect of glass modifier, shown in Fig.4.23. Here BaO and V_2O_5 are kept constant while Ag_2O is increasing and TeO_2 is decreasing from 35 to 0 mol % in the present series. The infrared absorption spectrum shows different bands at 1020, 964, 920, 894, 887, 850, 790, 650-750 cm^{-1} for different samples. The peak observed at 1020 cm^{-1} for all the samples with very low intensity is due to the vibrations of the non bridging V=O of the VO_5 group [22]. The broad band at 887 cm^{-1} for z=25 and 30 mol % samples, is assigned to ν_{asym} stretching vibrations of VO_3 terminal groups of the pyrovanadate ions which are formed by the condensation of VO_4^{-3} tetrahedra. This band is shifting towards high frequency continuously and acquires a position at 920 cm^{-1} for rest of the samples. The intensity of this peak increases sharply as modifier increases. The broad band in the frequency range of 650-750 cm^{-1} for z=25 and 30 mol % samples has been shifted slightly towards high frequency and splits into two small peaks at 669 and 790 cm^{-1} for z=50 mol % and 55 mol % samples. These peaks are assigned to the combined effect of vanadium and tellurium groups. It may be due to ν_{sym} vibrations of V-O-V group of vanadium

oxide (normally observed at around 620 cm^{-1}), TeO_4 groups (at around 667 cm^{-1}) [19] and TeO_3 groups (at 777 cm^{-1}) [20] of tellurium oxide.

A high intense band at 725 cm^{-1} in z=60 mol %, is assigned to ν_{sym} vibrations of V-O-V group because tellurium is absent in this particular sample. After z= 45 mol %, some new bands start forming at different positions e.g., at 850, 894, 964 cm^{-1}. These bands are assigned to ν_{asym} vibrations of V-O-V bonds involved in the corner sharing of VO_5 polyhedra [23], ν_{sym} vibrations of VO_3 terminal stretching of pyrovanadate ions and the high frequency band at 964 cm^{-1} is assigned to the symmetric stretching vibrations of VO_2 groups of VO_4 polyhedra. The position of these bands is not changing but their intensity increases with composition.

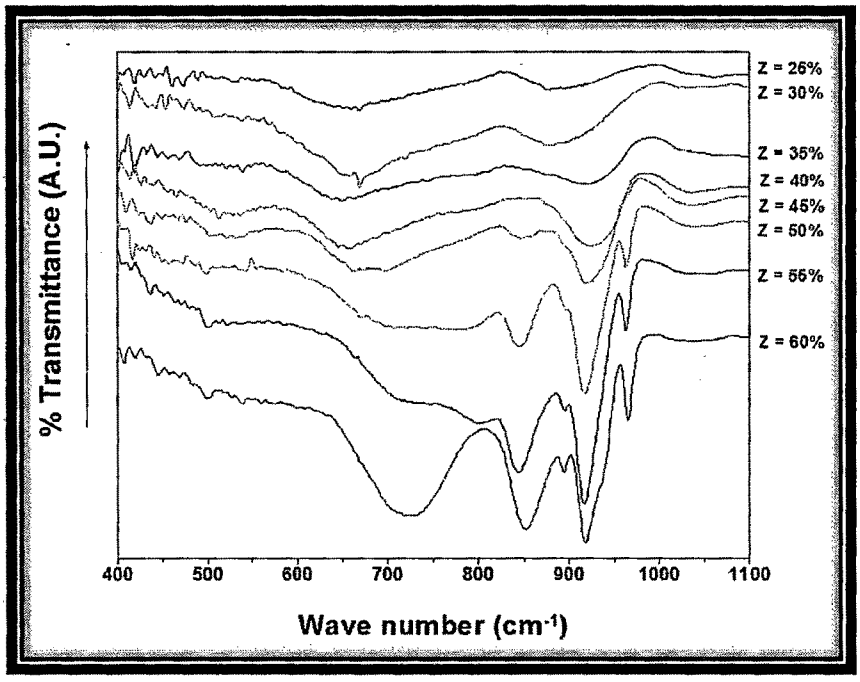

Fig.4.23. FTIR spectra of all samples of $5BaO\text{-}zAg_2O\text{-}35V_2O_5\text{-}(60\text{-}z)TeO_2$ series.

4.4 Transport number measurement by EMF method:

The silver ion transport number of the prepared quaternary glasses is found out by the EMF method. The emf value (E_{obs}) obtained for the samples at room temperature can be compared with the corresponding theoretical value (E_{theo}) of the open circuit voltage for Ag/I_2 couple i.e., 0.687 V. The open circuit voltage (OCV), silver ion transport number (t_{Ag}) and corresponding electronic transport number (t_e) are summarized in Table.4.1. It is clearly observed from the first series data that the silver ion transport number (t_{Ag}) is increasing with modifier increase combined with a decrease of V_2O_5 content. Fig. 4.24 shows the plot of

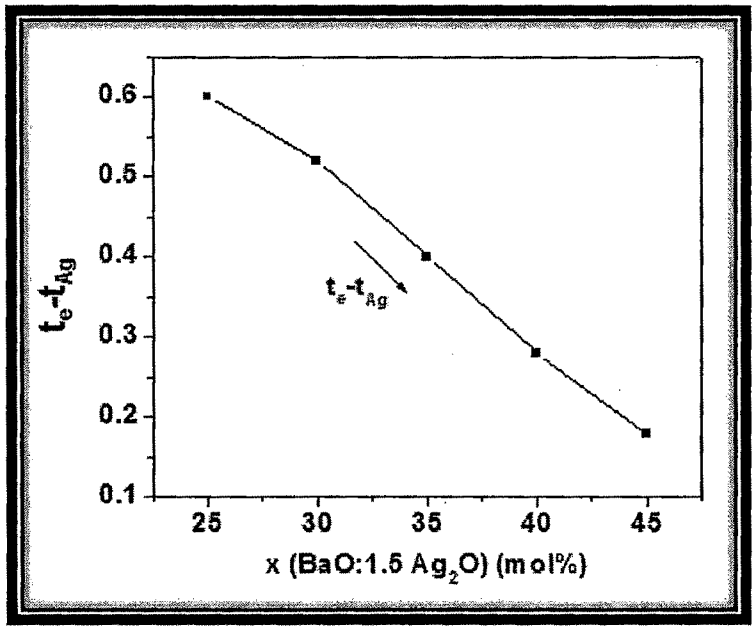

Fig.4.24. Difference between the electronic (t_e) and ionic transport number (t_{Ag}) for first series.

Table 4.1: OCV (open circuit voltage), silver ion transport number (t_{Ag}) and electronic transport number (t_e) for three series by EMF method.

Series	mole%	OCV (V)	t_{Ag}	t_e (=1-t_{Ag})
Series 1	x=			
	25	0.137	0.20	0.80
	30	0.165	0.24	0.76
	35	0.206	0.30	0.70
	40	0.247	0.36	0.64
	45	0.282	0.41	0.59
Series 2	y=			
	20	0.206	0.30	0.70
	25	0.288	0.42	0.58
	30	0.337	0.49	0.51
	35	0.412	0.60	0.40
	40	0.460	0.67	0.33
	45	0.508	0.74	0.26
	50	0.550	0.80	0.20
	55	0.611	0.89	0.11
Series 3	z=			
	25	0.378	0.55	0.45
	30	0.426	0.62	0.38
	35	0.467	0.68	0.32
	40	0.495	0.72	0.28
	45	0.522	0.76	0.24
	50	0.549	0.80	0.20
	55	0.570	0.83	0.17
	60	0.584	0.85	0.15

the difference between electronic and ionic transport number. It is clear from the figure that the electronic component is dominating in the series and the value (t_e-t_{Ag}) clearly decreases with the component.

Fig. 4.25 shows the same plot for second series where the electronic component is dominating for y=20-30 mol% and the value (t_e-t_{Ag}) decreases whereas for rest of the samples ionic component is dominating and the value i.e., (t_{Ag}-t_e) increases with composition. However, the correlation between V_2O_5 content and electronic conductivity is not simple. In this case, we have to take into account not only the V_2O_5 content alone but rather the concentration of aliovalent vanadium pairs (mainly V^{+4}/V^{+5}). That concentration depends on several factors as e.g., redox conditions during glass preparation process, concentration of the modifier (e.g., Ag_2O).

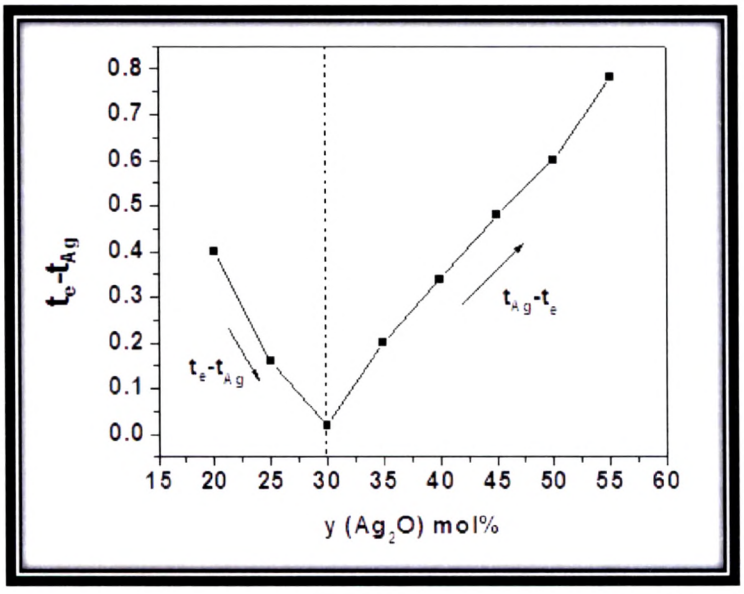

Fig.4.25. Difference between the electronic (t_e) and ionic transport number (t_{Ag}) for second series.

In the third series, it is clear from the Fig.4.26 that the ionic component is dominating in all the samples and the value (t_{Ag}-t_e) increases continuously. It appears from the above study that the samples are of mixed conducting nature. Other systems like Li_2O-V_2O_5-P_2O_5 [27], AgI-Ag_2O-V_2O_5-TeO_2 [28] and AgI-Ag_2O-V_2O_5-P_2O_5 [29] have also been reported which confirm mixed conducting nature of their samples by the transport number studies.

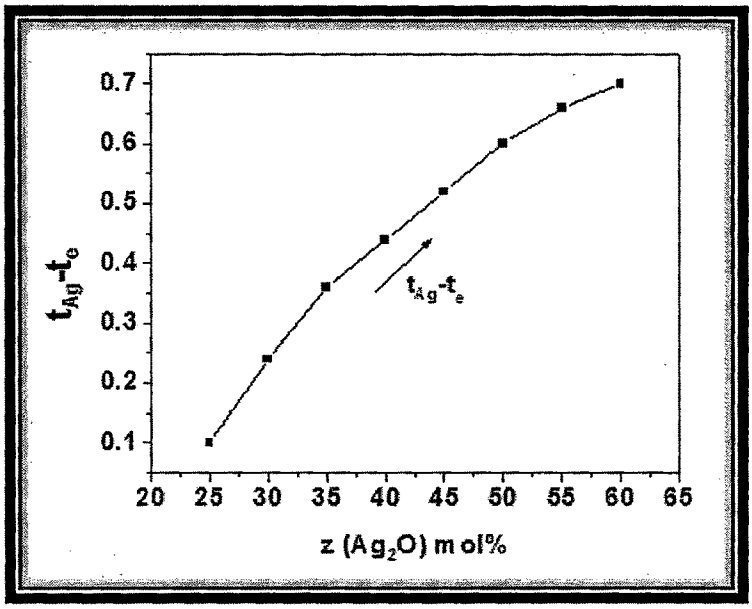

Fig.4.26. Difference between the electronic (t_e) and ionic transport number (t_{Ag}) for third series.

4.5 Density and Molar Volume:

Densities of all the glass samples were measured at room temperature by Archimedes's principle, using Eq. 3.2. Density is related to how tightly the ions

Table 4.2: Density and Molar Volume for three different series studied:

Series	mole%	Density (gm cm^{-3})	Molar Volume V_m (cm^3 mol^{-1})
Series 1	x=		
	25	3.72	49.83
	30	3.83	48.65
	35	4.02	46.55
	40	4.18	45.02
	45	4.39	43.07
Series 2	y=		
	20	3.89	48.34
	25	4.09	46.57
	30	4.35	44.36
	35	4.44	44.05
	40	4.66	42.44
	45	4.87	41.18
	50	5.22	38.89
	55	5.42	37.85
Series 3	z=		
	25	4.61	40.12
	30	4.73	39.91
	35	4.87	39.52
	40	4.98	39.38
	45	5.06	39.47
	50	5.19	39.12
	55	5.28	39.16
	60	5.31	39.58

and ionic groups are packed together in the sub structure. The measured values of the density and molar volume are given in the Table. 4.2. It is observed from the table that the increase of density of glass samples are lying in the range of 3.72 to 4.39 gm/cm^3 for first series, 3.89 to 5.42 gm/cm^3 for second series and 4.61 to 5.31 gm/cm^3 for third series.

From the density measurement, the number of ions per unit volume i.e., N_V and N_{Ag}, average spacing between the ions i.e., Ag-Ag spacing and V-V spacing and the molar volume that are useful for understanding conduction mechanism in these glasses were determined. These values are given in chapter 5. From the results of three different series, it is clear that increasing modifier content (BaO and Ag_2O) increases the density possibly due to the fact that Ba^{+2} and Ag^+ ions occupy interstitial positions in the glass network [30]. Similar behavior of density and molar volume is observed by other workers also [31, 32]. The relationship between density and composition of an oxide glass system can be expressed in terms of molar volume V_m which can be calculated from the density and composition using the formula reported in the Chapter-3 Eq. 3.3. It is also observed from the table that the molar volume V_m decreases with an increase of modifier content in first and second series while for third series it is almost constant with increasing modifier content. Drake et. al. [33] reported that the decrease of molar volume with modifier indicates that the topology of the network does not change with composition. The change in density can also be explained rather simply as due to the replacement of lighter cation (V) by heavier ones (Ba and Ag) [34, 35].

References:

[1] H. U. Beyeler, P. Bruesch and T. Hibma, Phys. Rev. B 18 9 (1978) 4570.

[2] Z. W. Wilchinsky, J. Appl. Phys. 15 (1944) 806.

[3] Y. Limb and R. F. Davis, J. Am. Ceram. Soc. 62 (1978) 403.

[4] S. Sen, A. Ghosh, J. Appl. Phys. 86 (1999) No.4 2078.

[5] S. Szu, F. S. Chang, Solid State Ionics 176 (2005) 2695.

[6] H. Sakata, K. Sega, Phys. Rev. B, 60 No.5 (1999) 3230.

[7] A.A. Bahgat, I.I. Shaltout and A.M. Abu-Elazm J. Non-Cryst. Solids 150 (1992) 179-184.

[8] J. Krogh-Moe, Phys. Chem. Glasses 6, No.2 (1965) 46.

[9] Y. Dimitriev, V. Dimitrov, M. Arnaudov, J. Mat. Sci. 18 (1983)1353.

[10] Y. Dimitriev, V. Dimitrov and M. Arnaudov, J. Mat. Sci. 14 (1979) 723.

[11] R. H. Doremus (1973), Glass Science, John Wiley & Sons, New York pg. 323.

[12] S. Sen, A. Ghosh, J. Non-Cryst. Solids 258 (1999) 29.

[13] S. Sen, A. Ghosh, J. Mater Res. 15 (2000) 995.

[14] V. Pimitrov, Y. Dimitiev, M. Arnaudov, D. Topalov, J. Non-Cryst. Solids 57 (1983) 147.

[15] J. T. Quan, C. F. Adams, J. Phys. Chem. 70 (1966) 331.

[16] T. K. Bansal, R. G. Mendiratta, Phys. Chem. Glasses 28, 6 (1987) 242.

[17] T. Sekiya, N. Mochida, A. Ohtsuka, M. Tonokawa, J. Non Cryst. Solids 144 (1992) 128-44.

[18] H. M. M. Moawad, H. Jain, R. El-Mallawany, T. Ramadan, M. El-Sharbiny, J. Am. Ceram. Soc. 85 (11) (2002) 2655-59.

[19] Manisha Pal, K. Hirota, Y. Tsujigami and H. Sakata, J. Phy. D: Appl. Phys. 34 (2001) 459.

[20] B. V. R. Chowdari, K. L. Tan, Ling Fang, Solid State Ionics 113 (1998) 711.

[21] Y. Dimitriv, V. Dimitriv, M. Arnaudov, D. Topalov, J. Non-Cryst. Solids 57 (1983)147.

[22] E. F. Lambson, G. A. Saunders, B. Bridge, R. El-Mallawany, J. Non-Cryst. Solids 69 (1984)117.

[23] H. G. Bachman, F. R. Ahmed, W.H. Barner, Z. Krstallogh 115 (1961) 110.

[24] S. Murugesan, A. Wijayasinghe, B. Bergman, Solid State Ionics 178 (2007) 779.

[25] S. Sindhu, S. Sanghi, A. Agarwal, Sonam, V. P. Seth, N. Kishore, Physica B 365 (2005) 65-75.

[26] A. K. Arof, S. Radhakrishna, J. Alloys and Compounds, 200 (1993) 129.

[27] P. Jozwiak, J. E. Garbarczyk, M. Wasiucionek, Mat. Sci.-Poland 24 (2006) 147-153.

[28] S. Jayaseelan, P. Muralidharan, M. Venkateswarlu, N. Satyanarayana, Mat. Sci. & Engg. B 119 (2005) 136-143.

[29] J. E. Garbarczyk, M. Wasiucionek, B. Wnetrzewski, W. Jakubowski, Phys. Stat. Sol. (a) 156 (1996) 441-449.

[30] R. H. Doremus, Glass Science, John Wiley & Sons, New York (1973) p. 178.

[31] A. Al-Hajry, A. Al-Shahrani, M. M. Desoky, Mat. Chem. Phys. 95 (2006) 300-306.

[32] M.M. El-Desoky, J. Non-Cryst. Solids 351 (2005) 3139-3146.

[33] C. F. Drake, J. A. Stephens, B. Yates, J. Non-Cryst. Solids 28 (1978) 61.

[34] S. Sen, A. Ghosh, J. Non-Cryst. Solids 258 (1999) 29.

[35] S. Sen, A. Ghosh, J. Mater. Res. 15 (2000) 995.